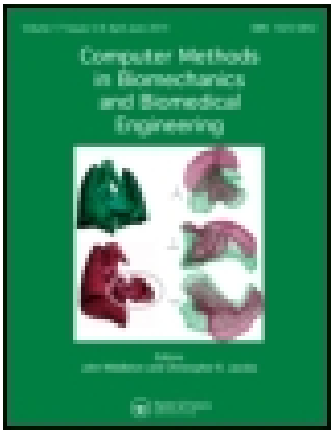

Computer Methods in Biomechanics and Biomedical Engineering

Publication details, including instructions for authors and subscription information:
http://www.tandfonline.com/loi/gcmb20

Virtual human hand: model and kinematics

Esteban Peña-Pitarch[a], Neus Ticó Falguera[b] & Jingzhou (James) Yang[c]

[a] Escola Politècnica Superior d'Enginyeria de Manresa (EPSEM-UPC), Manresa, Spain

[b] Althaia Xarxa Assistencial de Manresa, Manresa, Spain

[c] Human-Centric Design Research Laboratory, Texas Tech University, Lubbock, TX, USA

Published online: 24 Aug 2012.

Computer Methods in Biomechanics and Biomedical Engineering, 2014
Vol. 17, No. 5, 568–579, http://dx.doi.org/10.1080/10255842.2012.702864

Virtual human hand: model and kinematics

Esteban Peña-Pitarch[a]*, Neus Ticó Falguera[b] and Jingzhou (James) Yang[c]

[a]*Escola Politècnica Superior d'Enginyeria de Manresa (EPSEM-UPC), Manresa, Spain;* [b]*Althaia Xarxa Assistencial de Manresa, Manresa, Spain;* [c]*Human-Centric Design Research Laboratory, Texas Tech University, Lubbock, TX, USA*

(*Received 10 January 2012; final version received 11 June 2012*)

The human hand plays an important role in daily life. It is the interface between the human and the exterior world by positioning, orienting, touching and grasping objects. The human hand has multiple degrees of freedom (DOFs) to enable mobility and dexterity. A virtual human hand model can be inserted into CAD (Computer Aided Design) models to assess the manipulation capabilities in the early design stage to reduce design time and cost. Joystick assessment is one of the important design cases. This study is a first step towards a comprehensive hand simulation tool to simulate the manipulation and grasping of objects. This paper presents a novel 25 DOFs' hand skeletal model based on hand anatomy and hand kinematics: (1) joint range of motion, (2) Denavit–Hartenberg method to define the joint relationship and (3) finger workspace determination. Novelty for this hand model includes arching the palm with the four DOFs added in the carpometacarpal and wrist joints for the ring and small fingers.

Keywords: virtual human; virtual human hand; kinematics; simulation

1. Introduction

Virtual human modelling and simulation have gained significant momentum by incorporating humans into early stages of design to reduce the design time and cost. Virtual hand modelling and simulation are important parts of whole body modelling. The hand model is the foundation of a hand simulation tool that ensures accuracy in grasping. This paper is a first step towards the ultimate goal of developing a hand simulation tool for evaluation of products such as joysticks.

Significant research efforts have been dedicated to the hand in the past several decades. Some alternative hand models have been developed, and this paper proposes a high-fidelity hand model based on those models in the literature. The model proposed in this paper does not consider the wrist joint. To develop a realistic hand model, we followed Tubiana (1981), Kapandji (1996) and Tubiana et al. (1996), who provided detailed descriptions of taxonomy of the hand. Complete analysis and classification of the human hand were presented by Cutkosky (1989) for the design of hands for manufacturing tasks. Albrecht et al. (2003) showed a hand design without grasp simulation, and a database for hand grasping system was proposed by Aydin and Nakajima (1999). For simulating human fingers, Barbagli et al. (2004) presented a deformable model based on Hertzian theories. Analysis of finger motion coordination in the hand manipulative and gestic acts for the fingers except the thumb were studied by Braido and Zhang (2004). Based on postural synergies, Santello et al. (1998) suggested that hand posture may be regulated independently of the control of the contact forces that are used to grasp an object.

Other studies on the virtual hand include the DaibaHand in several papers of Miyata et al. (2004, 2005, 2006, 2007). This hand model is based on optical motion capture. For the virtual human called MAN3D, Savescu et al. (2004) developed a virtual hand with 25 degrees of freedom (DOFs) including the wrist. Based on visual recognition, Nolker and Ritter (2002) reconstructed a hand posture in the articulated hand model with 20 DOFs. Devices with a high number of DOFs are very complex for controlling and performing activities. To avoid these difficulties, Rijpkema and Girard (1991) proposed coupling the movements of some joints and reduced the number of DOFs. Based on three functions of grasping surfaces, namely object-supporting, pressing and wrapping functions, Saito and Nagata (1999) presented a study to assist robot designers in producing innovative robotic hand systems. The Sharmes simulator is a highly realistic human hand and forearm model (Chalfoun et al. 2005). The model contains 38 muscles and 24 DOFs. Two of these DOFs are for the wrist, 2 are for the arm and the 20 DOFs are for hand.

Medical studies related to the human hand were also considered. For index finger movements, Darling and Cole (1990) and Darling et al. (1994) determined whether dynamic interaction torques are significant for the control of digit movements and investigated whether such torques are compensated by specific muscle activation patterns. Measuring the ability of humans to discriminate the orientations of cylinders by passively contacting the fingerpad was discussed by Dodson et al. (1998).

*Corresponding author. Email: esteban.pena@upc.edu

To determine whether other digits move when normal humans attempt to move just one digit, Hager-Ross and Schieber (2000) recruited 10 right-handed subjects to move one finger at a time while they recorded the motion of all five digits simultaneously with both a video motion analysis system and an instrumented glove. Kamojima et al. (2004) proposed a system that identifies the position and orientation of hand bones using magnetic resonance volume images by registration of a bone model. A study to determine a distribution of the forces produced by motor unit activity in the human flexor digitorum profundus was conducted by Kilbreath et al. (2002). Park et al. (2003) studied the application of the Fibonacci sequence to the anatomy of the human hand. A review of visual interpretation of hand gestures for human–computer interaction was presented by Pavlovic et al. (1997), Valero-Cuevas (2000), Valero-Cuevas et al. (2003) and Pearlman et al. (2004). Valero Cuevas (2005) studied hand muscles related to hand motion and manipulation. Yokogawa and Hara (2002) investigated whether distribution patterns of the maximum fingertip force in all directions from 0° to 360° around the index fingertip are the same among subjects. Li and Zhang (2009, 2010) presented a new computational framework for biodynamic modelling of human movement and attempted to elucidate the roles of the flexors. A probabilistic biodynamic model of the index finger was constructed to estimate the muscle–tendon forces during an experimentally measured index finger flexion movement.

This paper presents a comprehensive study about hand modelling and simulation based on our previous studies Peña Pitarch et al. (2005a, 2005b). In the meantime, we are working on joint torque, finger posture prediction and autonomous grasping capabilities. The ultimate goal is to develop a hand simulation tool for product design.

This paper is organised as follows: Section 2 reviews the hand anatomy. Section 3 introduces the 25 DOFs hand model formulated using the Denavit–Hartenberg (D–H) method. Then, forward and inverse kinematic analysis is studied in Section 4, and workspace analysis is investigated in Section 5. Discussion is give in Section 6. Finally, conclusions are given in Section 7.

2. Anatomy of the hand

The hand has 27 bones; 8 bones are located in the wrist, 3 are located in the thumb (1 metacarpal and 2 phalanx) and 4 metacarpal and 12 phalanxes are located in the other fingers. Each bone is connected with another by different kinds of joints. There are two basic joints, condylar and troqueal joints. Therefore, each finger has different movements based on different types of joints.

Figure 1 shows the definition of movements for each finger in terms of flexion/extension (F/E) and abduction/adduction (Ab/Ad) and the visual concept of hyper-extension (Tubiana et al. 1996). This explains the phenomenon of the finger extending beyond its natural maximum upward direction.

Tables 1 and 2 show the range of motion for fingers (Tubiana et al. 1996), where H means hyper-extension, IP is the interphalangeal joint, DIP is the distal interphalangeal joint and PIP is the proximal interphalangeal joint. Figure 2 shows the movements of the thumb; for the proposed model, the movements of opposition and retroposition are simulated by the sum of the movements of the carpometacarpal (CMC) and metacarpophalangeal (MCP) joints.

3. Kinematic hand model

Based on the anatomy of the hand, a 25 DOFs hand model was developed. Four DOFs are located in the CMC joint for both the ring and small fingers to provide the palm arc motion. The thumb has five DOFs, and both the index and middle fingers have four DOFs (the MCP joint has two, and the PIP and DIP joint have one each). The D–H method is implemented because each finger is considered a

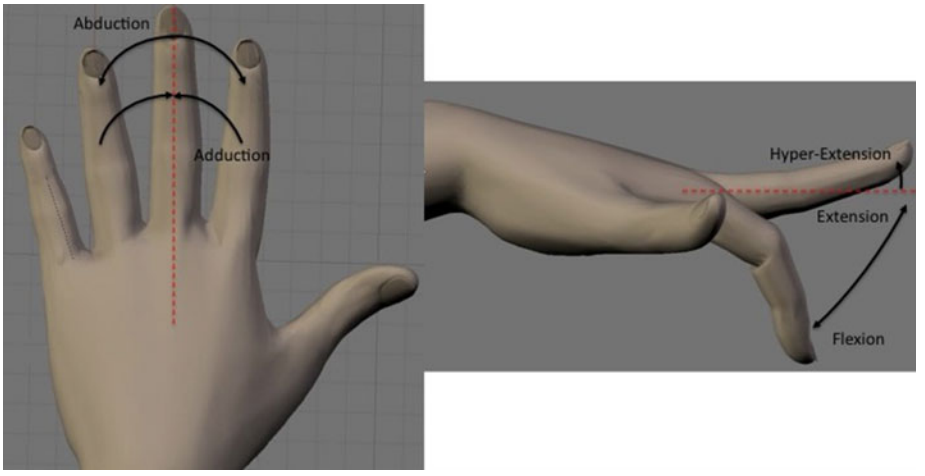

Figure 1. Abduction/adduction (Ab/Ad) and flexion/extension (F/E).

Table 1. Range of motion of the thumb (in degrees).

CMC	Adduction/abduction	0(contact)/60
CMC	Extension/flexion	25/35
MCP	Extension/flexion	10H/55
MCP	Adduction/abduction	0/60
IP	Extension/flexion	15H/80

Table 2. Range of motion for the index, middle, ring and small fingers (in degrees).

Finger	MCP (E/F)	PIP (E/F)	DIP (E/F)	MCP (Ab/Ad)
Index	0/80	0/100	10H/90	13/42
Middle	0/80	0/100	10H/90	8/35
Ring	0/80	0/100	20H/90	14/20
Small	0/80	0/100	30H/90	19/33

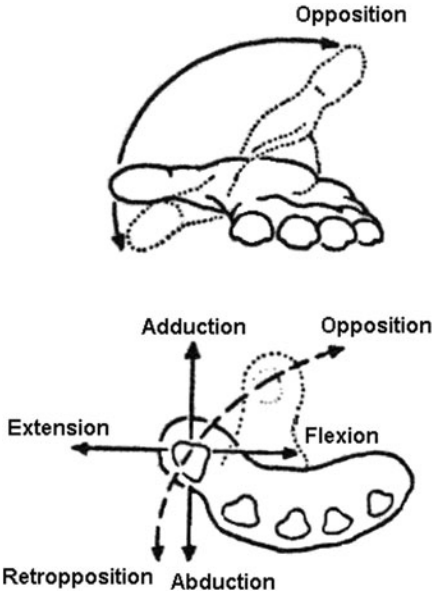

Figure 2. Abduction/adduction and flexion/extension of the thumb.

ray, i.e. an open chain, with revolute joints. The D–H tables for fingers will be set up, and forward and inverse kinematics will be implemented. $[q_1 \dots q_{25}]^{\mathrm{T}}$ denotes joint angles for the right hand and $[q_{26} \dots q_{50}]^{\mathrm{T}}$ those for the left hand. Figure 3 shows a posterior view of the right hand, and Figure 4 shows a palmar view of the left hand.

The D–H convention in Denavit and Hartenberg (1955) becomes necessary because we have five open-loop chains and a high number of DOFs. First, we define the local and global coordinate systems. Second, the hand model with 25 DOFs is justified in the hand anthropometry section. Next, the transformation from local to global coordinates is analysed.

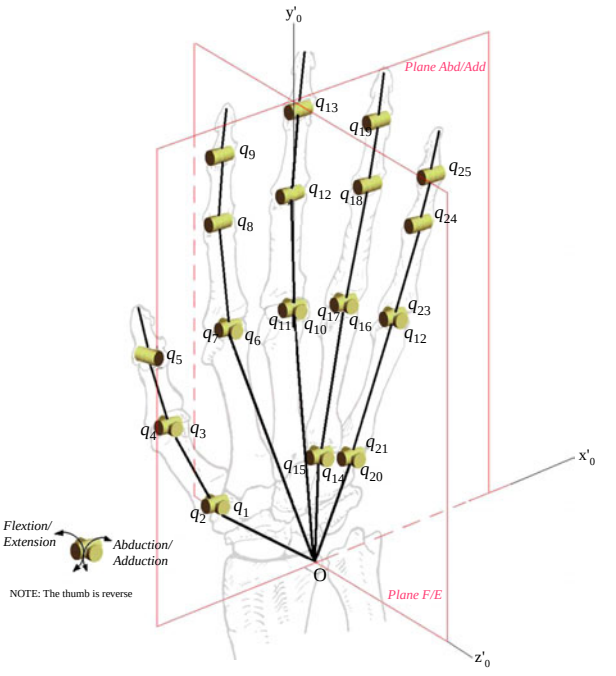

Figure 3. The 25 DOFs hand. Posterior view of the right hand.

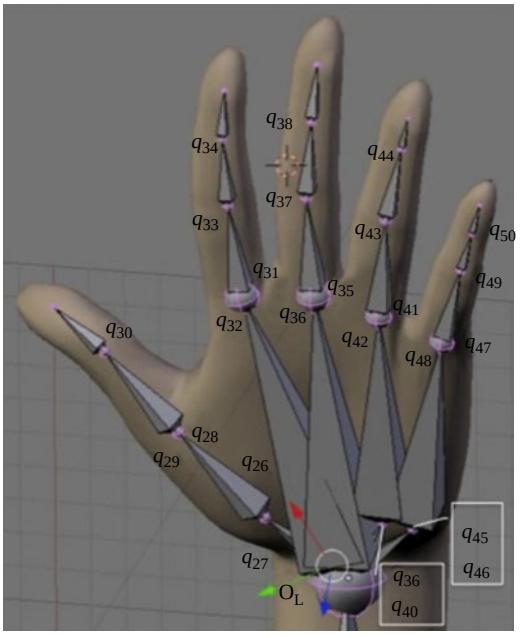

Figure 4. The 25 DOFs hand. Palmar view of the left hand.

3.1 *Global and local coordinates (frames)*

Each ray has a root (local frame) located at points O_1, O_2, O_3, O_4, O_5 and the local frames are defined by $x_1y_1z_1$, $x_2y_2z_2$, $x_3y_3z_3$, $x_4y_4z_4$ and $x_5y_5z_5$ as shown in Figure 5, respectively. The global frame is located at the wrist joint centre (point O) and is represented by $x_0y_0z_0$. In Figure 5, γ_j $(j = 1 \dots 5)$ are defined as angles between

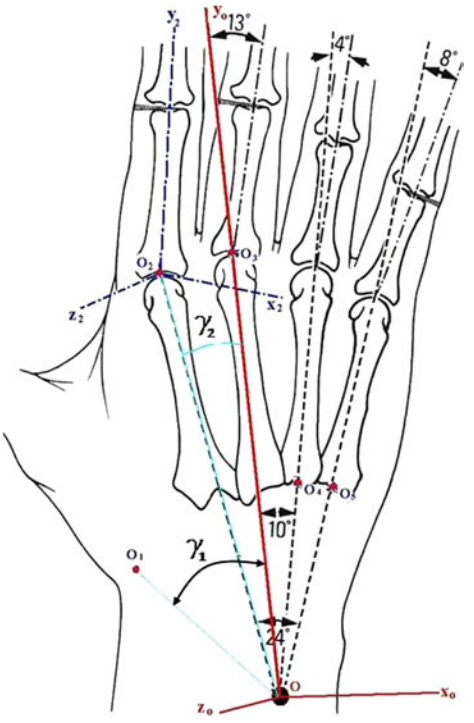

Figure 5. Local and global coordinate systems.

line OO_j to the axis y_o. In general, γ_j are defined as $\gamma_1 = 40°$, $\gamma_2 = 7°$, $\gamma_3 = 13°$, $\gamma_4 = 14°$ and $\gamma_5 = 25°$. In addition, to distinguish the left-hand and right-hand coordinate systems, a subscript L is added for the left hand and a subscript R for the right hand.

3.2 Hand anthropometry

Figure 6 shows the two parameters defining the bones' length. These parameters, hand length (HL) and hand breadth (HB), are different for every person.

Figure 7 shows the segment lengths for the four fingers $i =$ II, III, IV, V, where the notations II, III, IV, V denote the index finger, middle finger, ring finger and small finger,

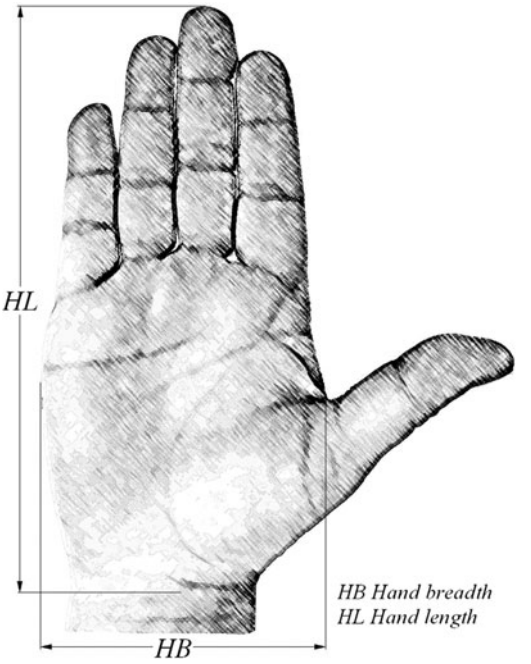

Figure 6. Parametric lengths for a hand.

respectively. ℓ_{i-0}, ℓ_{i-1}, ℓ_{i-2}, ℓ_{i-3} and ℓ_{i-4} are, respectively, the lengths from the global coordinate system (point O) to the local coordinate system (O_1, O_2, O_3, O_4, O_5), the lengths of the metacarpal bones, the lengths of the proximal phalanx bones, the lengths of the medial phalanx bones and the lengths of the distal phalanx bones. Figure 8 shows the segment lengths for the thumb, where $i =$ I (Buchholz et al. 1992; Sancho-Bru 2000).

Table 3 shows the length formula for the metacarpal bones. Table 4 shows the length formula for the phalangeal bones. The segment lengths are used as parameters in the D–H calculation and are consequently used in the kinematic model. Once all segment lengths for each finger are obtained, we can build the open-loop chain and the D–H table for each finger. D–H tables are given in Appendix.

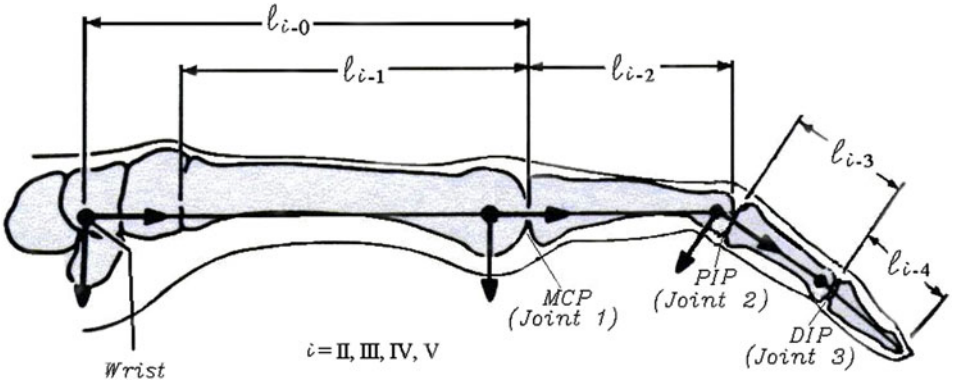

Figure 7. Finger segment lengths.

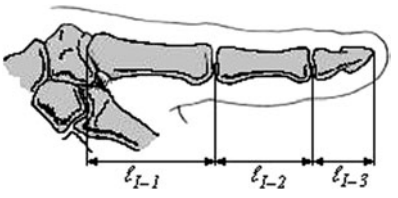

Figure 8. Thumb segment lengths.

Table 3. Length formula for the metacarpal bones.

	Metacarpal bones	
Thumb	$0.251 \times \mathrm{HL}$	$\ell_{\mathrm{I}-1}$
Index	$\sqrt{(0.374 \times \mathrm{HL})^2 + (0.126 \times \mathrm{HB})^2}$	$\ell_{\mathrm{II}-1}$
Middle	$0.373 \times \mathrm{HL}$	$\ell_{\mathrm{III}-1}$
Ring	$\sqrt{(0.336 \times \mathrm{HL})^2 + (0.077 \times \mathrm{HB})^2}$	$\ell_{\mathrm{IV}-1}$
Small	$\sqrt{(0.295 \times \mathrm{HL})^2 + (0.179 \times \mathrm{HB})^2}$	$\ell_{\mathrm{V}-1}$

Table 4. Length formula for the phalangeal bones.

	Proximal		Middle		Distal	
Thumb	$0.196 \times \mathrm{HL}$	$\ell_{\mathrm{I}-2}$	–	–	$0.158 \times \mathrm{HL}$	$\ell_{\mathrm{I}-3}$
Index	$0.265 \times \mathrm{HL}$	$\ell_{\mathrm{II}-2}$	$0.143 \times \mathrm{HL}$	$\ell_{\mathrm{II}-3}$	$0.097 \times \mathrm{HL}$	$\ell_{\mathrm{II}-4}$
Middle	$0.277 \times \mathrm{HL}$	$\ell_{\mathrm{III}-2}$	$0.170 \times \mathrm{HL}$	$\ell_{\mathrm{III}-3}$	$0.108 \times \mathrm{HL}$	$\ell_{\mathrm{III}-4}$
Ring	$0.259 \times \mathrm{HL}$	$\ell_{\mathrm{IV}-2}$	$0.165 \times \mathrm{HL}$	$\ell_{\mathrm{IV}-3}$	$0.107 \times \mathrm{HL}$	$\ell_{\mathrm{IV}-4}$
Small	$0.206 \times \mathrm{HL}$	$\ell_{\mathrm{V}-2}$	$0.117 \times \mathrm{HL}$	$\ell_{\mathrm{V}-3}$	$0.093 \times \mathrm{HL}$	$\ell_{\mathrm{V}-4}$

3.3 *Transformation from local frames to the global frame*

In the virtual human environment, when a virtual human grasps or manipulates an object, there are two steps to achieve this task. The first step is to predict the upper body posture. The second step is to predict individual finger posture with the wrist position and orientation as inputs. In Figure 5, the hand segment formed by points $O, O_1, O_2, O_3, O_4, O_5$ is a rigid body, and the root of each ray has different locations. Therefore, all fingers should have a common coordinate system. We use the global coordinate system as the common coordinate system for all fingers. It is necessary to transform all local coordinate systems to the global coordinate system.

To demonstrate the procedure of transforming the local coordinate to the global coordinate system, the thumb of the left hand is used as one example. For other fingers, the procedure is similar.

Figure 9 shows the local frame $x_{1\mathrm{L}}y_{1\mathrm{L}}z_{1\mathrm{L}}$ where the distance $\ell_{Io} = 0.118\mathrm{HL}$ (Buchholz et al. 1992; Sancho-Bru 2000). From Figure 9, we can define vectors $\mathbf{x}_{1\mathrm{L}}$, $\mathbf{y}_{1\mathrm{L}}$ and $\mathbf{z}_{1\mathrm{L}}$ for the local frame with respect to the global frame

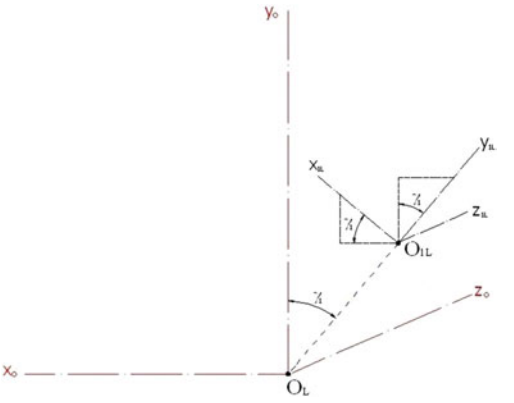

Figure 9. Local and global frames for the left thumb.

$x_{0\mathrm{L}}y_{0\mathrm{L}}z_{0\mathrm{L}}$:

$$\mathbf{x}_{1\mathrm{L}} = \begin{bmatrix} \cos\gamma_1 \\ \sin\gamma_1 \\ 0 \end{bmatrix}, \quad \mathbf{y}_{1\mathrm{L}} = \begin{bmatrix} -\sin\gamma_1 \\ \cos\gamma_1 \\ 0 \end{bmatrix}, \quad \mathbf{z}_{1\mathrm{L}} = \begin{bmatrix} 0 \\ 0 \\ 1 \end{bmatrix}.$$

The vector $\mathbf{s}$ formed from point O_{L} to point $O_{1\mathrm{L}}$ is defined as

$$\mathbf{s} = \begin{bmatrix} -\ell_{Io}\sin\gamma_1 \\ 0 \\ \ell_{Io}\cos\gamma_1 \end{bmatrix}.$$

Finally, the transformation matrix for the left thumb is obtained using Equation (1):

$$ {}^{0}H_1 = \begin{bmatrix} \mathbf{x}_{1\mathrm{L}} & \mathbf{y}_{1\mathrm{L}} & \mathbf{z}_{1\mathrm{L}} & \mathbf{s} \\ 0 & 0 & 0 & 1 \end{bmatrix} = \begin{bmatrix} \cos\gamma_1 & -\sin\gamma_1 & 0 & -\ell_{Io}\sin\gamma_1 \\ \sin\gamma_1 & \cos\gamma_1 & 0 & 0 \\ 0 & 0 & 1 & \ell_{Io}\cos\gamma_1 \\ 0 & 0 & 0 & 1 \end{bmatrix}. \quad (1)$$

Working in a similar way, one can obtain other transformation matrices.

4. Forward and inverse kinematics

4.1 *Finger end-effector equations*

In this study, the end-effector refers to a fingertip. In this section, the finger end-effector equations are derived based on above local to global frame transformation matrices and D–H method (Angeles 2002).

The position vector of an end-effector is defined by $\mathbf{p}(\mathbf{q}^i)$ with respect to a finger's local frame by

$$\begin{bmatrix} \mathbf{p}(\mathbf{q}^i) \\ 1 \end{bmatrix} = {}^0A_1^1A_2 \ldots {}^{n-1}A_n \begin{bmatrix} 0 \\ 0 \\ 0 \\ 1 \end{bmatrix},$$

where $\mathbf{q}^i = [q_1 \ldots q_n]^{\mathrm{T}}$, $i = \mathrm{I}, \mathrm{II}, \mathrm{III}, \mathrm{IV}, \mathrm{V}$ and n represents the total DOFs for a specific finger. A_i are defined in Appendix. With the application of the homogeneous transformation matrix, one can obtain:

$${}^0T_i = {}^0A_1\,{}^1A_2 \ldots {}^{n-1}A_n = \begin{bmatrix} n_x & o_x & p_x & d_x \\ n_y & o_y & p_y & d_y \\ n_z & o_z & p_z & d_z \\ 0 & 0 & 0 & 1 \end{bmatrix}, \quad (2)$$

where the vector $\mathbf{d} = [d_x\, d_y\, d_z]^{\mathrm{T}}$ is the position of the fingertip with respect to finger's local frame.

Therefore, the position vector with respect to the global frame is defined by

$$\begin{bmatrix} \mathbf{w}(\mathbf{q}^i) \\ 1 \end{bmatrix} = [{}^0\mathrm{H}_i] \begin{bmatrix} \mathbf{p}(\mathbf{q}^i) \\ 1 \end{bmatrix}. \quad (3)$$

4.2 *Forward kinematics*

An interface has been developed in Visual Basic to demonstrate hand forward kinematics shown in Figure 10. The inputs include HB, HL and all joint angles. The outputs are the end-effector positions. The bottom of the interface shows the fingertip positions in the global coordinate system.

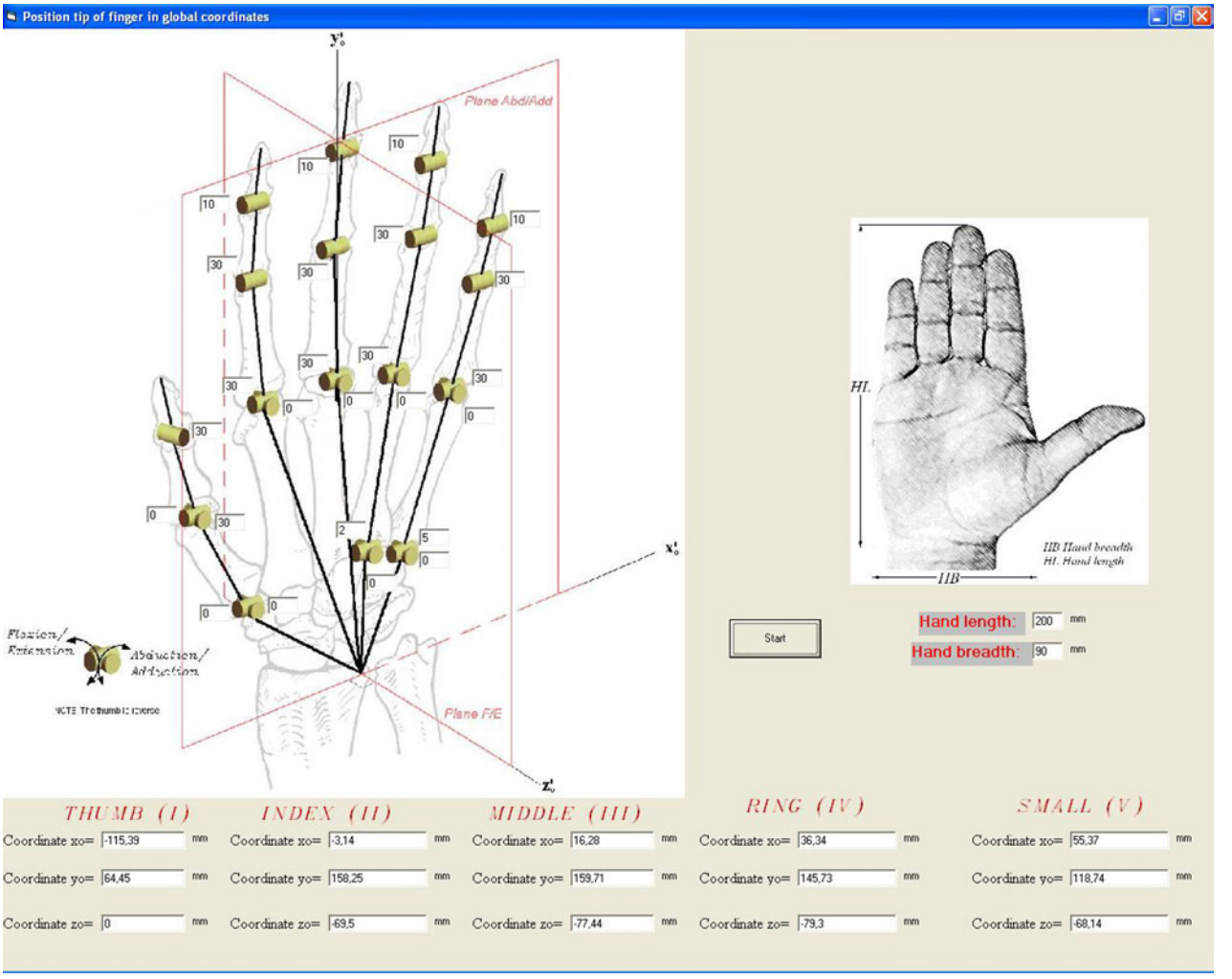

Figure 10. Interface for forward kinematic.

4.3 Inverse kinematics

When the positions of the end-effectors are given, the unknowns are the finger joint angles in Equation (3). In general, the inverse kinematics problem has multiple solutions due to mechanism redundancy. However, the maximum number for one ray of hand is six DOFs. The hand has some natural restrictions (i.e. the DIP joint cannot hyperextend 100°), and the feasible space is really small. Therefore, one unique solution can be approximately obtained.

To implement the inverse kinematics algorithm, a method from robotics theory was adapted. The method requires the number of unknowns to be the same as the number of equations. Finally, it solves a set of highly nonlinear equations. The Newton–Raphson (N–R) method was implemented for four DOFs, five DOFs and six DOFs individual fingers. However, for some configurations, the system of equations did not converge. Through the test, we found that the starting point for N–R method is critical to ensure convergence. To ensure the N–R method convergence, we implemented the steepest descent method to determine a reasonable starting point before we solved the nonlinear equations.

In this section, one example of the index finger is used to illustrate the procedure of the inverse kinematics. The index finger has four DOFs, and to solve inverse kinematics, the theory of robotics provided in Angeles (2002) was used, where

$$ {}^{0}T_4 = {}^{0}A_1 \cdot {}^{1}A_2 \cdot {}^{2}A_3 \cdot {}^{3}A_4, \tag{4} $$

and from Equation (4)

$$ {}^{0}T_4 = \begin{bmatrix} n_x & o_x & p_x & d_x \\ n_y & o_y & p_y & d_y \\ n_z & o_z & p_z & d_z \\ 0 & 0 & 0 & 1 \end{bmatrix}, $$

where the position vector $\mathbf{d} = [\,-11.22 \quad 152.341 \quad 77.4\,]^{\mathrm{T}}$ is known and the equation of the transformation matrices is defined as

$$ {}^{0}A_1 = \begin{bmatrix} \cos\left(q_6+\frac{\pi}{2}\right) & -\cos\left(-\frac{\pi}{2}\right)\sin\left(q_6+\frac{\pi}{2}\right) & \sin\left(-\frac{\pi}{2}\right)\sin\left(q_6+\frac{\pi}{2}\right) & 0 \\ \sin\left(q_6+\frac{\pi}{2}\right) & \cos\left(-\frac{\pi}{2}\right)\cos\left(q_6+\frac{\pi}{2}\right) & -\sin\left(-\frac{\pi}{2}\right)\cos\left(q_6+\frac{\pi}{2}\right) & 0 \\ 0 & \sin\left(-\frac{\pi}{2}\right) & \cos\left(-\frac{\pi}{2}\right) & 0 \\ 0 & 0 & 0 & 1 \end{bmatrix}, $$

$$ {}^{1}A_2 = \begin{bmatrix} \cos q_7 & -\cos 0 \sin q_7 & \sin 0 \sin q_7 & \ell_{\mathrm{II}-1}\cos q_7 \\ \sin q_7 & \cos 0 \cos q_7 & -\sin 0 \cos q_7 & \ell_{\mathrm{II}-1}\sin q_7 \\ 0 & \sin 0 & \cos 0 & 0 \\ 0 & 0 & 0 & 1 \end{bmatrix}, $$

$$ {}^{2}A_3 = \begin{bmatrix} \cos q_8 & -\cos 0 \sin q_8 & \sin 0 \sin q_8 & \ell_{\mathrm{II}-2}\cos q_8 \\ \sin q_8 & \cos 0 \cos q_8 & -\sin 0 \cos q_8 & \ell_{\mathrm{II}-2}\sin q_8 \\ 0 & \sin 0 & \cos 0 & 0 \\ 0 & 0 & 0 & 1 \end{bmatrix}, $$

$$ {}^{3}A_4 = \begin{bmatrix} \cos q_9 & -\cos 0 \sin q_9 & \sin 0 \sin q_9 & \ell_{\mathrm{II}-3}\cos q_9 \\ \sin q_9 & \cos 0 \cos q_9 & -\sin 0 \cos q_9 & \ell_{\mathrm{II}-3}\sin q_9 \\ 0 & \sin 0 & \cos 0 & 0 \\ 0 & 0 & 0 & 1 \end{bmatrix}. $$

The unknowns are the angles q_6, q_7, q_8 and q_9. Therefore, the system of equations has four equations and four unknowns. The solution was obtained as $\mathbf{q} = [\,q_6 \quad q_7 \quad q_8 \quad q_9\,]^{\mathrm{T}}$ by solving the equation.

5. Workspace analysis

This section shows the formulation for generating the workspace for each finger, beginning with Jacobian methods and the row-rank deficiency criteria. Then, based on the singular sets, the finger workspace is visualised using *Mathematica*^{R}.

5.1 Formulation

The idea of a singular *Jacobian* is used to identify all barriers inside and on the boundary of the workspace. Because the Jacobian is non-square, we define such barriers as a subset of the workspace at which the Jacobian of the constraint function of $\mathbf{H}_q = \partial\mathbf{H}\partial\mathbf{q}$ is *row-rank deficient* (Abdel-Malek and Othman 1999), i.e. barriers are defined by ∂W and are characterised by

$$ \partial W \subset \left\{ \mathrm{Rank}\,\mathbf{H}_{q^*} \cdot (\mathbf{q}^*) < k, \quad \text{for some } \mathbf{q}^* \text{ with } \mathbf{H}(\mathbf{q}^*) = 0 \right\}, \tag{5} $$

where k is at least $(3 + n - 1)$. Because of the form of the Jacobian characterised by Equation (5), three distinct conditions arise as follows:

(a) *Type I singularity sets.* If no joints have reached their limits, the diagonal sub-matrix $\mathbf{q}_\lambda$ is full of row rank. Therefore, the only possibility for $\mathbf{H}_{q^*}$ to be row-rank deficient is when the block matrix $\mathbf{x}_q$ is row-rank deficient. Type I singularity set is defined as

$$ S^{(1)} \equiv \left\{ \mathbf{p} \in \mathbf{q} : \mathrm{Rank}\,[\mathbf{x}_q] < 3, \quad \text{for some constant subset of } \mathbf{q}^* \right\}, \tag{6} $$

where $\mathbf{p}$ is within the specified joint limit constraints and may contain joints that are functions of others or constant values.

(b) *Type II singularity sets.* When certain joints reach their limits, e.g. $\partial\mathbf{q}^{\mathrm{lim}} = [q_i^{\mathrm{limit}}, q_j^{\mathrm{limit}}, q_k^{\mathrm{limit}}]^{\mathrm{T}}$, the corresponding diagonal elements in the matrix will be equal to

zero. Therefore, the corresponding matrix is subjected to the rank-deficiency criterion, in which it will take on the following form:

$$\mathbf{H}_{q^*} \approx \begin{bmatrix} \mathbf{x}_{q_1} & \dots & \mathbf{x}_{q_i} & \mathbf{x}_{q_j} & \mathbf{x}_{q_k} & \dots & \mathbf{x}_{q_n} \\ 0 & \dots & 1 & 0 & 0 & \dots & 0 \\ 0 & \dots & 0 & 1 & 0 & \dots & 0 \\ 0 & \dots & 0 & 0 & 1 & \dots & 0 \end{bmatrix} \quad (7)$$

and in which the three columns pertaining to $\mathbf{x}_{q_i}$, $\mathbf{x}_{q_j}$ and $\mathbf{x}_{q_k}$ are removed such that the rank deficiency criteria are applied again. From the foregoing observation, the second type of singular sets is formulated. Define a new vector $\partial\mathbf{q}^{\text{lim}} = [q_i^{\text{limit}}, q_j^{\text{limit}}, q_k^{\text{limit}}]^{\text{T}}$, which is a sub-vector of $\mathbf{q}$ where

$$1 \le \dim\left(\partial\mathbf{q}^{\text{limit}}\right) \le (n-3).$$

Type II singularity set is defined as

$$\begin{aligned} &\{\mathbf{p} = [\hat{\mathbf{p}} \cup \partial\mathbf{q}^{\text{limit}}] : \text{Rank}\ [\mathbf{x}_{\mathbf{q}}(\mathbf{w}, \partial\mathbf{q}^{\text{limit}})] < 3, \\ &\text{for some}\ \hat{\mathbf{p}} \in \mathbf{q}^*,\ \dim(\partial\mathbf{q}^{\text{limit}}) \le (n-3)\}, \end{aligned} \quad (8)$$

where $\hat{\mathbf{p}}$ is the singular set as a result of applying the rank deficiency criteria to Equation (7).

(c) *Type III singularity sets.* These are all sets that are composed of the combination of joints at their limits and are defined by

$$S^{(3)} \equiv \left\{\mathbf{p} \in \mathbf{R}^{(n-2)} : \mathbf{p} \equiv \partial\mathbf{q}^{\text{limit}} = \left[q_i^{\text{limit}}, q_j^{\text{limit}}, \dots\right]\right\}, \quad (9)$$

where $i \neq j$.

5.2 Finger workspace visualisation

In order to simplify the model without losing generality, the algorithm for the thumb is presented, and then we can extend it to other fingers. Note that each finger's workspace is visualised independently to avoid confusion when all workspaces of fingers are combined.

Section 5.1 showed the model and D–H table for the fingers. For the thumb, the range of motion is defined in Table 5.

Table 5. Range of motion of thumb (degrees).

	Min	Max
q_1	0	60
q_2	−25	35
q_3	0	60
q_4	−10	55
q_5	−15	80

5.2.1 Singularity set

Since $\Phi_{\mathbf{q}^*}$ is a 3×5 matrix, there are $n!/(3!(n-3)!) = 5!/(3!2!) = 10$ equations to be simultaneously solved, which represent the determinants of all square 3×3 sub-Jacobians. There are three sets of solutions:

(I) As a result of solving the equations generated by the sub-Jacobians, the rank deficiency of $\Phi_{\mathbf{q}^*}$ is a 3×5 matrix which yields $s_1 = \{q_3 = 0, q_4 = 0, q_5 = 0\}$.
(II) The second singularity set can be obtained by substituting two joint limits into the Jacobian and solving the determinant of the sub-Jacobian excluding the column corresponding to the joint limit.
(III) The third set occurs when three of the variables reach their constraint limits. There are a total of 80 singular surfaces. In order to carry out this symbolic manipulation, a computer code using Mathematica was developed.

When all of the singular surfaces are plotted together, the boundary will be obtained, as shown in Figures 11 and 12.

By implementing the same procedure as used for the thumb, we can obtain the workspace of the index finger. Note that the index and middle fingers have similar kinematic models. Each finger has four DOFs, but the dimensions are different. Therefore, here we only show the workspace of the index finger as in Figures 13 and 14.

Similarly, the ring and small fingers have the same kinematic models, and we only show the workspace of the ring finger in Figures 15 and 16.

6. Discussion

This paper proposed a novel virtual hand model that includes 25 DOFs where each finger has two revolute

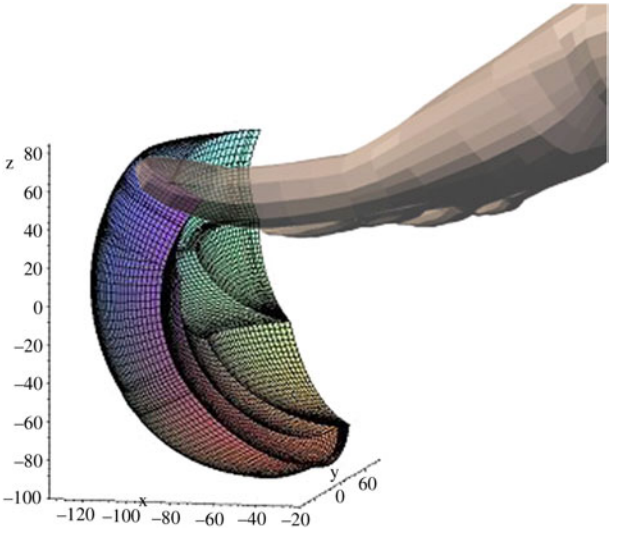

Figure 11. One view of the workspace for the thumb.

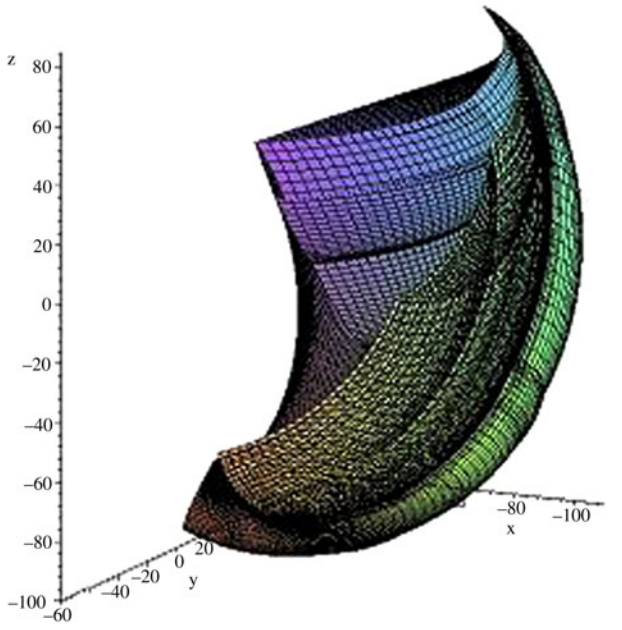

Figure 12. Another view of the workspace for the thumb.

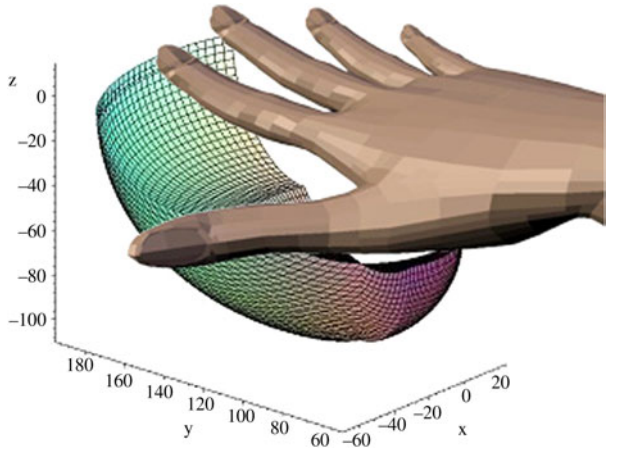

Figure 13. One view of the workspace for the index finger.

joints located in the CMC joints. These four revolute joints ensure that the proposed virtual hand has the capability of arching palm. This is the highest number of DOFs for hand models in the literature. Therefore, the proposed hand model is much closer to the real human hand.

The D–H method is the foundation of the proposed hand model and the kinematics. This inherent characteristic ensures that the hand model can be changeable with the input hand breath and length to adapt to different people's hands. This means that the proposed hand model can present any person's hand just by inputting the corresponding hand parameters.

Forward and inverse kinematics have been proposed and it is convenient to have a user friendly interface to

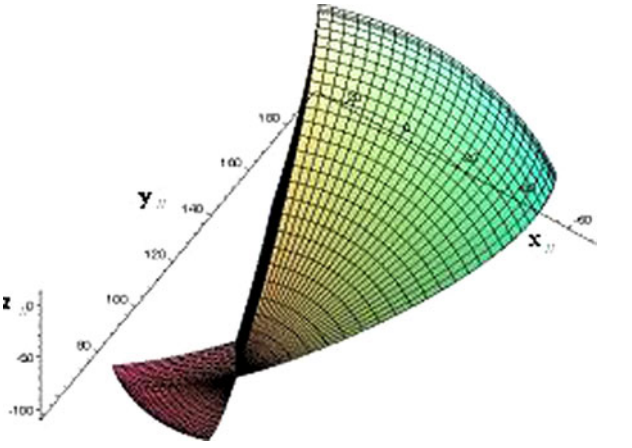

Figure 14. Another view of the workspace for the index finger.

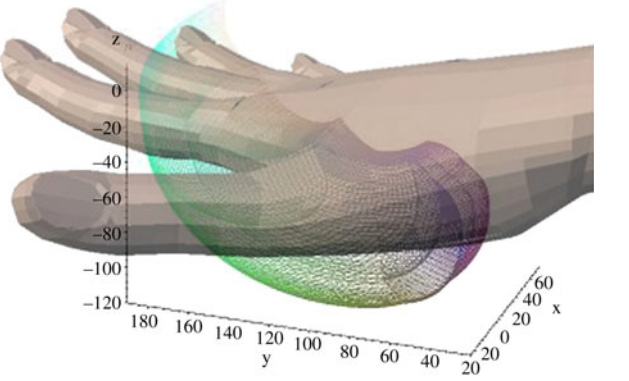

Figure 15. One view of the workspace for the ring finger.

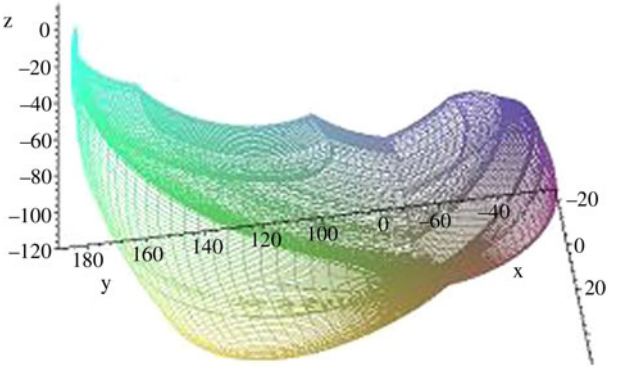

Figure 16. Another view of the workspace for the ring finger.

operate the hand model. In addition, the finger reach envelopes have been developed for various applications such as joystick button reachability check.

The limitation of the proposed hand model is that it does not include muscles. This limits the hand model's usefulness in finger force and fatigue analysis.

7. Conclusions

In this paper, a novel 25 DOFs hand model was proposed. With this model, the transformation of coordinates from the local to global frame was derived. The D–H method was applied for each finger. All fingers within one hand finally have a common global frame located on the wrist joint centre. Forward and inverse kinematics algorithms were implemented. Jacobian rank deficiency method was used to determine and visualise the finger workspace. The advantages of this hand model include (1) high fidelity, (2) variable anthropometry because the D–H method was implemented, (3) intuitive visualisation of forward and inverse kinematics and (4) intuitive workspace visualisation.

Projects for other different hand capabilities are ongoing. These capabilities include joint torque determination, autonomous grasping, voxel-based finger reach envelope, a comprehensive hand interface, hand comfort metrics, and a combination of hand and upper body. The ultimate goal is to develop a user-friendly hand simulation suite that can be used to assess joystick design and other tasks that involve hand manipulation and grasping.

During the hand modelling and simulation project, we realised that the human hand is complicated, and it is not an easy task to model this mechanism accurately, although significant research efforts have been made on hand modelling and simulation in the digital human modelling community. Note that none of the hand models currently available in the literature are realistic and high fidelity. Future work includes validation of the proposed model using experiment and grasping, although we have made great progress on grasping research. Hand grasping is a challenging task because it is really difficult to develop a hand model that is exactly the same as the real hand mechanism (ideal structure of high dexterity and mobility). In addition, the shapes of objects to be grasped are arbitrary, and it is difficult to have a unique approach to autonomously grasp any object. We believe that hand-grasping research still has a long way to go. Also, other future work will be (1) developing a muscular skeletal hand model, (2) understanding the carpal tunnel syndrome by using the muscular model and (3) studying hand vibration responses for hand tool design.

Acknowledgement

This study was partially supported by the Spanish Government with the project DPI2010-15446.

References

Abdel-Malek K, Othman S. 1999. Multiple sweeping using the Denavit–Hartenberg representation method. Comput Aided Des. 31(9):567–583.

Albrecht I, Haber J, Seidel HP. 2003. Construction and animation of anatomically based human hand models. In: Eurographics/SIGGRAPH symposium on computer animation, San Diego, CA, USA. p. 1–12.

Angeles J. 2002. Fundamentals of robotic mechanical systems: theory, methods, and algorithms. Mechanical Engineering Series, 2nd ed, Springer-Verlag, New York.

Aydin Y, Nakajima M. 1999. Database guided computer animation of human grasping using forward and inverse kinematics. Comput Graph. 23(1):145–154.

Barbagli F, Frisoli A, Salisbury K, Bergamasco M. 2004. Simulating human fingers: a soft finger proxy model and algorithm. In: HAPTICS '04. Proceedings of the 12th International Symposium on Haptic Interfaces for Virtual Environment and Teleoperator Systems, Chicago, Il, USA. p. 9–17.

Braido P, Zhang X. 2004. Quantitative analysis of finger motion coordination in hand manipulative and gestic acts. Hum Mov Sci. 22:661–678.

Buchholz B, Armstrong T, Goldstein S. 1992. Anthropometric data for describing the kinematics of the human hand. Ergonomics. 35(3):261–273.

Chalfoun J, Younes R, Renault M, Ouezdou F. 2005. Forces, activation and displacement prediction during free movement in the hand and forearm. J Robot Syst. 22(11):653–660.

Cutkosky M. 1989. On grasp choice, grasp models, and the design of hands for manufacturing tasks. IEEE Trans Robot Automat. 5(3):269–279.

Darling WG, Cole KJ. 1990. Muscle activation patterns and kinetics of human index finger movements. J Neurophysiol. 65(5):1098–1108.

Darling WG, Cole KJ, Miller GF. 1994. Coordination of index finger movements. J Biomech. 27(4):479–491.

Denavit J, Hartenberg R. 1955. A kinematic notation for lower-pair mechanisms based on matrices. J Appl Mech. 22: 215–221.

Dodson MJ, Goodwin AW, Browning AS, Gehring HM. 1998. Peripheral neural mechanisms determining the orientation of cylinders grasped by the digits. J Neurosci. 18(1):521–530.

Hager-Ross C, Schieber MH. 2000. Quantifying the independence of human finger movements: comparisons of digits, hands, and movement frequencies. J Neurosci. 20(22): 8542–8550.

Kamojima S, Miyata N, Ota J. 2004. Identification of position and orientation of hand bones from MR images by bones model registration. In: Proceedings of the IEEE International Intelligent Robots and Systems, Sendai, Japan. p. 2021–2027.

Kapandji I. 1996. Fisiologia articular. Miembro superior. 5th ed.. Madrid: Medica Panamericana.

Kilbreath SL, Gorman RB, Raymond J, Gandevia SC. 2002. Distribution of the forces produced by motor unit activity in the human flexor digitorum profundus. J Physiol (Lond). 543(1):289–296.

Li K, Zhang X. 2009. A novel two-stage framework for musculoeskeletal dynamic modeling: an application to multifingered hand movement. IEEE Trans Biomed Eng. 56(7):1949–1957.

Li K, Zhang X. 2010. A probabilistic finger biodynamic model better depicts the roles of the flexors during unloaded flexion. J Biomech. 43(13):2618–2624.

Miyata N, Kouchi M, Kurihara T, Mochimaru M. 2004. Modeling of human hand link structure from optical motion capture data. In: IROS 2004. Proceedings of the IEEE/RSJ International Conference on Intelligent Robots and Systems, Sendai, Japan. Vol. 3. p. 2129–2135.

Miyata N, Kouchi M, Mochimaru M. 2006. Posture estimation for design alternative screening by DhaibaHand – cell phone operation. In: SAE 2006 Digital Human Modeling for Design and Engineering Conference. p. 2006-01-2327 (CD–ROM). SAE Technical Paper 2006-01-2327, 2006, doi:10.4271/2006-01-2327, Lyon, France.

Miyata N, Kouchi M, Mochimaru M. 2007. Generation and validation of 3D links for representative hand models. SAE Technical Paper 2007-01-2512, 2007, doi:10.4271/2007-01-2512. Seatle, Usa.

Miyata N, Mochimaru M, Kouchi M, Kawachi K, Kurihara T. 2005. Hand link modeling and motion generation from motion capture data based on 3D joint kinematics. In: SAE 2005 Digital Human Modeling for Design and Engineering Conference. p. 2005-01-2687 (CD–ROM), Iowa City, USA.

Nolker C, Ritter H. 2002. Visual recognition of continuous hand postures. IEEE Trans Neural Netw. 13(4):983–994.

Park AE, Fernandez JJ, Schmedders K, Cohen MS. 2003. The fibonacci sequence: relationship to the human hand. J Hand Surg. 28(1):157–160.

Pavlovic V, Sharma R, Huang T. 1997. Visual interpretation of hand gestures for human-computer interaction: a review. IEEE Trans Pattern Anal Mach Intell. 19(7):677–695.

Pearlman JL, Roach SS, Valero-Cuevas FJ. 2004. The fundamental thumb-tip force vectors produced by the muscles of the thumb. J Orthop Res. 22(2):306–312.

Peña Pitarch E, Yang J, Abdel-Malek K. 2005a. SANTOSTM hand: a 25 degrees of freedom model. In: Proceedings of SAE Digital Human Modeling for Design and Engineering, Iowa City, USA, June.

Peña-Pitarch E, Yang J, Abdel-Malek K. 2005b. SANTOSTM Hand: Workspace Analysis. In: Proceedings of the IASTED Conference on Modelling and Simulation., May 18–25. Cancun, Mexico.

Rijpkema H, Girard M. 1991. Computer animation of knowledge-based human grasping. Comp Graph. 25(4):339–348.

Saito F, Nagata K. 1999. Interpretation of grasp and manipulation based on grasping surfaces. In: Proceedings of the IEEE International Conference on Robotics and Automation, Kyongju, Korea. Vol. 2. p. 1247–1254.

Sancho-Bru X. 2000. Model biomecanic de la ma orientat al disseny d'eines manualsUniversitat Jaume I. PhD Thesis. ISBN-9788469146712.

Santello M, Flanders M, Soechting JF. 1998. Postural hand synergies for tool use. J Neurosci. 18(23):10105–10115.

Savescu AV, Cheze L, Wang X, Beurier G, Verriest JP. 2004. A 25 degrees of freedom hand geometrical model for better hand attitude simulation. SAE International conference and exposition of Digital Human Modeling for Design and Engineering, June 14–16, 2004, Oakland University, Rochester, Michigan, USA. SAE paper 2004-01-2196.

Tubiana R. 1981. The hand. Vol. I 2nd ed. W.B. Saunders Company (ISBN: 0721689078 / 0-7216-8907-8) Saint Louis, Missouri, USA.

Tubiana R, Thomine J, Mackin E. 1996. Examination of the hand and wrist. 2nd ed. Martin Dunitz. ISBN: 1853175447/1-85317-544-7. Publisher: Informa Healthcare.

Valero-Cuevas FJ. 2005. An integrative approach to the biomechanical function and neuromuscular control of the fingers. J Biomech. 38(4):673–684.

Valero-Cuevas FJ. 2000. Predictive modulation of muscle coordination pattern magnitude scales fingertip force magnitude over the voluntary range. J Neurophysiol. 83(3):1469–1479.

Valero-Cuevas FJ, Johanson M, Towles JD. 2003. Towards a realistic biomechanical model of the thumb: the choice of kinematic description may be more critical than the solution method or the variability/uncertainty of musculoskeletal parameters. J Biomech. 36:1019–1030.

Yokogawa R, Hara K. 2002. Measurement of distribution of maximum index-fingertip force in all directions at fingertip in flexion/extension plane. J. Biomech. Eng. 124:302–307.

Appendix A

The transformation matrix A_i, where subscript $i = 1 \ldots 25$, is shown below:

$$ {}^{i-1}A_i = \begin{bmatrix} \cos\theta_i & -\cos\alpha_i \sin\theta_i & \sin\alpha_i \sin\theta_i & a_i \cos\theta_i \\ \sin\theta_i & \cos\alpha_i \cos\theta_i & -\sin\alpha_i \cos\theta_i & a_i \sin\theta_i \\ 0 & \sin\alpha_i & \cos\alpha_i & d_i \\ 0 & 0 & 0 & 1 \end{bmatrix} $$

The D–H parameters are shown in Tables A1–A5.

Table A1. Thumb D–H table.

	θ_i	d_i	a_i	α_i
1	$q_1 + (\pi/2)$	0	0	$-\pi/2$
2	q_2	0	$\ell_{\mathrm{I}-1}$	$\pi/2$
3	q_3	0	0	$-\pi/2$
4	q_4	0	$\ell_{\mathrm{I}-2}$	$\pi/2$
5	q_5	0	$\ell_{\mathrm{I}-3}$	$-\pi/2$

Table A2. Index D–H table.

	θ_i	d_i	a_i	α_i
6	$q_6 + (\pi/2)$	0	0	$-\pi/2$
7	q_7	0	$\ell_{\mathrm{II}-2}$	0
8	q_8	0	$\ell_{\mathrm{II}-3}$	0
9	q_9	0	$\ell_{\mathrm{II}-4}$	0

Table A3. Middle D–H table.

	θ_i	d_i	a_i	α_i
10	$q_{10} + (\pi/2)$	0	0	$-\pi/2$
11	q_{11}	0	$\ell_{\mathrm{III}-2}$	0
12	q_{12}	0	$\ell_{\mathrm{III}-3}$	0
13	q_{13}	0	$\ell_{\mathrm{III}-4}$	0

Table A4. Ring D–H table.

	θ_i	d_i	a_i	α_i
14	$q_{14} + (\pi/2)$	0	0	$-\pi/2$
15	q_{15}	0	$\ell_{\mathrm{IV}-1}$	$\pi/2$
16	q_{16}	0	0	$-\pi/2$
17	q_{17}	0	$\ell_{\mathrm{IV}-2}$	0
18	q_{18}	0	$\ell_{\mathrm{IV}-3}$	0
19	q_{19}	0	$\ell_{\mathrm{IV}-4}$	0

Table A5. Small D–H table.

	θ_i	d_i	a_i	α_i
20	$q_{20} + (\pi/2)$	0	0	$-\pi/2$
21	q_{21}	0	$\ell_{\mathrm{V}-1}$	$\pi/2$
22	q_{22}	0	0	$-\pi/2$
23	q_{23}	0	$\ell_{\mathrm{V}-2}$	0
24	q_{24}	0	$\ell_{\mathrm{V}-3}$	0
25	q_{25}	0	$\ell_{\mathrm{V}-4}$	0